Research Square

Preprints are preliminary reports that have not undergone peer review.
They should not be considered conclusive, used to inform clinical practice,
or referenced by the media as validated information.

Acoustic transmission through the human middle ear from infrasonic to audible frequencies: a computational biomechanics study

Ismael OUZZINE
Aix Marseille Univ, APHM, CNRS, IUSTI, La Conception University Hospital
Ralph HADDAD
Aix Marseille Univ, APHM, CNRS, IUSTI, La Conception University Hospital
Lionel MEISTER
IUSTI, Aix Marseille Univ
Thomas RADULESCO
Aix Marseille Univ, APHM, CNRS, IUSTI, La Conception University Hospital
Justin MICHEL
Aix Marseille Univ, APHM, CNRS, IUSTI, La Conception University Hospital
Sebastian HALM
University of Bern
Dario EBODE
Aix Marseille Univ, APHM, CNRS, IUSTI, La Conception University Hospital
Stéphane GARGULA
stephane.gargula@ap-hm.fr

Aix Marseille Univ, APHM, CNRS, IUSTI, La Conception University Hospital

Research Article

Keywords: middle ear, stapes, finite-volume modeling, acoustic transmission, infrasound

Posted Date: February 26th, 2026

DOI: https://doi.org/10.21203/rs.3.rs-8848413/v1

License: This work is licensed under a Creative Commons Attribution 4.0 International License.
Read Full License

Additional Declarations: No competing interests reported.

Abstract

The human middle ear acts as a frequency-dependent acoustic transmission system coupling sound pressure to inner-ear fluid motion. While its behavior has been extensively studied in the audible range, its response to infrasonic stimulation remains poorly characterized. Here, three middle-ear configurations were simulated using finite-volume modeling: a simplified structural model, a fluid–structure interaction model including a cochlear fluid domain, and an anatomically realistic model reconstructed from micro–computed-tomography data. Harmonic pressure excitations (4–4000 Hz; 70–120 dB sound-pressure levels) were applied to the tympanic membrane, and stapes displacement was quantified at the oval window. Across all models, a linear relationship between sound intensity and stapes displacement was observed. Similar amplitudes were obtained with and without cochlear fluid loading, indicating limited inertial coupling. Resonance-like behavior emerged in the mid-audible range and was consistent with published numerical predictions. Parametric analysis identified tympanic-membrane diameter and thickness, together with annular-ligament morphology, as the main determinants of amplitude variability, whereas footplate and oval-window geometry had negligible influence. These findings demonstrate that middle-ear acoustic transmission remains linear and continuous from infrasonic to low-audible frequencies, supporting simplified boundary conditions in acoustic and cochlear models involving low-frequency sound exposure.

I. INTRODUCTION

From an acoustics perspective, the middle ear functions as a pressure-to-displacement transformer whose frequency response shapes sound transmission to the cochlea. Efficient drug delivery to the inner ear remains a significant challenge in treating cochlear lesions, a major cause of disability worldwide[1–3]. The inaccessibility of the inner ear and the lack of substantial cochlear fluid movement pose considerable obstacles to this delivery[4,5]. Recent studies have suggested that harnessing hydrodynamic phenomena within the cochlea could enhance drug diffusion[5–7]. Ungar et al. demonstrated that exposure to a 30 dB sound wave at 512 Hz increased drug concentrations in rat perilymph[8]. Furthermore, a "steady streaming" phenomenon could facilitate perilymph mixing and drug diffusion within the cochlea[9,10]. Flaherty et al. also observed that very low-frequency stimulation (2 and 4 Hz) of the round window in guinea pigs can generate perilymphatic flow[11].

Several numerical models, mostly finite-element formulations, have been employed to predict the dynamic behavior of the middle ear, including stapes movement[12–16]. These models have provided valuable insights into the frequency response of the middle ear, notably showing that stapes displacement slightly increases from 100 to 1000 Hz, then decreases significantly from 1000 to 8000 Hz[17]. However, these studies have primarily focused on audible frequencies, leaving the infrasound domain (frequencies below 20 Hz) unexplored. To our knowledge, no prior human middle-ear model has systematically extended simulation below the auditory threshold while maintaining physiologic scaling of sound intensity and displacement.

We hypothesize that very low-frequency sound stimulations can generate stapes movements and induce perilymph movements potentially beneficial for drug distribution. This hypothesis is based on previous observations regarding the impact of low frequencies on cochlear flows but has never been specifically tested for infrasound in humans.

The primary objective of this study is to model middle ear transmission and stapes movement in humans in response to sound stimulations, particularly in the infrasound range. To achieve this, we developed a finite-volume–based numerical model of the human middle ear, based on accurate anatomical data and realistic mechanical properties of tissues. This model was used to simulate the stapes response to sound stimulations ranging from infrasound to audible frequencies.

This work represents an initial step towards understanding hydrodynamic phenomena in the cochlea in response to infrasound.

II. METHODS

A. Overview of modeling approach

Three complementary models were therefore developed: (i) a simplified configuration enabling controlled parametric analyses, (ii) a fluid–structure interaction configuration derived from the simplified model and including a perilymphatic domain to quantify cochlear loading, and (iii) an anatomical geometry reconstructed from histological sections to assess the effect of geometric realism. This tiered approach was chosen instead of a single fully detailed model to disentangle the respective roles of cochlear fluid loading and anatomical complexity.

Numerical simulations were performed using a finite-volume formulation implemented in Star-CCM+ (Siemens). The middle-ear system was modeled as a pressure-driven acoustic transmission system, with harmonic sound-pressure excitation applied to the tympanic membrane. Although thin shells are often treated with FEM formulations, the present study employed three-dimensional solid elements for the tympanic membrane, with strong local mesh refinement to ensure multiple elements through the thickness.

The fluid domain was represented as a quiescent Newtonian fluid with water-like density and viscosity, using no-slip boundary conditions at the cochlear walls and at the stapes footplate. Under these conditions, the fluid formulation captures viscous damping and inertial loading without introducing bulk flow or convective effects.

Solid mechanics of the ossicular chain and tympanic membrane were solved using a finite-volume solid formulation, and fluid–structure interaction was implemented to account for acoustic coupling between the middle-ear structures and the cochlear fluid domain. The simulations therefore focus on frequency-dependent acoustic transmission rather than on flow-driven fluid dynamics.

B. Simplified mechanical model

Based on the work of Gan et al.[12,14,17], we created an initial simplified middle ear model representing the ossicular chain as a total ossicular prosthesis, analogous to surgical ossiculoplasty (Fig. 1).

Table I presents the physical and mechanical characteristics (dimensions, density, Young's modulus) of this simplified model and an ossicular prosthesis.

Table I: characteristics of the 1st simplified model (solid): Material properties were primarily taken from Gan et al. (2004) for ossicles and tympanic membrane; ligament properties were adapted from Homma et al. (2009) [14,18]

	Eardrum	Disc prosthesis on eardrum	Prosthesis stem	Disc on oval window	Oval window (ellipse)	Ligament
Diameter	10mm	2mm	0,2mm	1mm	Large : 3mm Small 1,2mm	Width 0,08mm
Thickness	0,1mm	0,1mm		0,1mm	0,5mm	0,25mm
Length			4mm			
Density (kg/m^3)	1200	2200	2200	2200	2200	1200
Poisson's Ratio	0.48	0,3	0,3	0,3	0,3	0.48
Young's Modulus (Pa)	$2x10^7$	$1,41x10^{10}$	$1,41x10^{10}$	$1,41x10^{10}$	$1,41x10^{10}$	$2x10^5$

This model comprises six main components: the tympanic membrane, a prosthetic disk placed on the tympanum, a prosthetic stem, a disk on the oval window, the oval window itself (modeled as an ellipse), and the annular ligament. In the simplified configuration, secondary suspensory ligaments and ossicular joints were not modeled. Instead, the ossicular chain was represented as a single continuous elastic structure connected to the tympanic membrane and annular ligament. This choice was made to reduce the number of degrees of freedom and to isolate the influence of membrane and annular-ligament stiffness in parametric analyses.

C. Fluid–structure interaction (FSI) model

To study the influence of fluid-structure interactions on the mechanical response of the middle ear, we developed a second model (Fig. 2) based on our initial model.

This new model, designated as the FSI (Fluid-Structure Interaction) model, incorporates a liquid component following the oval window, thus representing the cochlear fluid load. The FSI model retains

the geometry and mechanical properties of the initial model for the solid part.

The main modification lies in the addition of a fluid domain adjacent to the oval window. The perilymph was modeled as an incompressible Newtonian fluid with viscosity comparable to water ($\mu \approx 1$ mPa·s). No-slip boundary conditions were applied not only at the stapes–fluid interface but also along all cochlear-duct walls. This configuration generates viscous shear throughout the entire fluid volume, resulting in distributed viscous damping in addition to classical added-mass effects. Because the cochlear domain represents a relatively large 3D volume compared with the solid-only models, discretization of this additional space required several times more control volumes, even with similar local mesh sizing. The interface between the solid domain (stapes) and the fluid domain was defined as a coupled boundary, allowing the transmission of forces and displacements between the two media. Cochlear loading was modeled through an explicit perilymphatic fluid domain extending from the oval window to the round window. The round-window termination was represented as a compliant membrane with the properties listed in **Table II**, and no additional radiation or absorbing boundary condition was imposed.

Table II: characteristics of the Cochlea and the round window of the 2nd FSI model. based on Gan et al. 2004 and Nakajima et al. 2009 [14,19]

	Cochlea	Round window
Diameter	3,4mm	1,6mm
Thickness		0,5mm
Length	70mm	
Density (kg/m^3)	1000	2200
Poisson's Ratio		0.48
Young's Modulus (Pa)		3.5x10^5

Although impedance or lumped-parameter boundary conditions can be used to approximate cochlear loading at the stapes footplate, we deliberately implemented an explicit volumetric perilymphatic domain in this study in order to capture distributed viscous dissipation and added-mass effects and to provide a reference solution for future reduced-order modeling.

This FSI approach allows for consideration of the loading effects of the cochlear fluid on middle ear dynamics, particularly the phenomena of added mass and viscous damping. The comparison between the initial purely solid model and the FSI model aims to quantify the impact of these fluid-structure interactions on the transmission of vibrations through the middle ear and to the cochlea.

D. Anatomical model

Finally, we developed a third model (Fig. 3), designated as the "anatomical model," based on a high-resolution CT image of the human middle ear.

We based our work on Halm et al.'s 2021 study, which provided access to their 3D reconstructions obtained by manual segmentation. This model was extracted by micro-CT from a human temporal bone embalmed using the Thiel method and stained with iodine for 3D modeling[20]. This anatomical representation therefore exhibits substantially higher geometric fidelity than the simplified configuration, including spatially varying tympanic-membrane thickness and detailed ligament morphology. The mechanical properties of the different structures were assigned in consistency with those used in our two previous models (Table I).

The suspensory ligaments of the ossicles were modeled, but incudo-malleolar and incudo-stapedial joints were represented as continuous linear elastic connections instead of modeling the cartilage layers explicitly. This anatomical model, for which no cochlear fluid component has been implemented, aims to evaluate the impact of the precise geometry of the ossicles and ligaments on the transmission of acoustic vibrations. For all three models, we opted for tetrahedral meshing, allowing faithful representation of the complex geometries of the ossicles and tympanic membrane, offering good adaptation to irregular shapes while maintaining acceptable mesh quality.

E. Simulation parameters and boundary conditions

To address the objective of our study, we applied vibrations to the tympanic membrane over a wide range of frequencies, from 4 Hz to 4000 Hz, thus covering most of the audible spectrum and extending into the infrasound domain. Particular emphasis was placed on very low frequencies (4, 8, 12, and 20 Hz). Although infrasonic stimulation is the primary focus of this study, simulations up to 4 kHz were performed to verify that the models reproduced well-established middle-ear transfer functions in the audible range before extrapolating to lower frequencies. A harmonic pressure load was applied uniformly over the lateral surface of the TM. Frequencies ranged from 4 to 4000 Hz; intensities from 70 to 120 dB SPL. The stimulation was applied as: $p\left(t\right) = p_0 \sin\left(2\pi\ ft\right)$, with $p_0$derived from the SPL. Stimulations were performed at different sound intensities (70, 80, 90, 100, 110, and 120 dB) for each tested frequency for solid models. Multiple sound-pressure levels were simulated to verify that the predicted response remained proportional to excitation amplitude across the investigated range and to ensure that no numerical or geometric nonlinearities arose within the tested conditions. A probe was placed at the center of the medial face of the stapes footplate, from which we collected the displacement during stimulation. Because apparent resonance-related oscillations produced cycle-to-cycle amplitude variations, the response was quantified using a mean steady-state displacement amplitude computed over several excitation periods rather than relying on a single maximum peak-to-peak value. This approach was selected to better reflect the overall mechanical energy transmitted by the system. As the FSI model required considerably more computing time, only 5 frequencies at 2 intensities were simulated. Frequencies above 4000 Hz were not tested in our research, which primarily focused on low frequencies. The tympanic annulus was rigidly fixed. The footplate edge was constrained by the annular

ligament. No prestress was applied to the tympanic membrane, and no-slip conditions were imposed at all fluid–solid interfaces. These simplifying assumptions were adopted to limit the number of poorly constrained parameters and follow common practice in middle-ear modeling. The perilymphatic domain extended from the oval window to the round window, which was modeled as a compliant membrane (Table 2). No additional radiation or absorbing boundary condition was imposed. Time-steps were 1/(200f), ensuring ≥ 200 steps per cycle. Convergence tolerance was 1×10^{-6} for residuals.

F. Computational environment and mesh-related computational load

All simulations were executed on the Aix-Marseille University high-performance computing facility (MésoCentre AMU), using between 32 and 160 CPU cores depending on node availability. The two solid-only configurations (prosthesis-like and anatomical) contained approximately 3.9 million and 3.8 million cells, respectively, and exhibited similar computational demand: each frequency–intensity condition, corresponding to 50 simulated cycles, required about 2 hours on 32 CPU cores.

The fluid–structure interaction configuration was markedly more demanding due to the presence of a full perilymphatic fluid domain and the need to resolve coupled solid–fluid dynamics at low frequencies. This model comprised approximately 5 million cells and was run on 160 CPU cores. A single frequency–intensity simulation required about 6 days to compute 20 cycles, reflecting both the larger volumetric mesh and the numerical cost of the FSI coupling scheme.

G. Data extraction and analysis

Using a custom Python script, peak-to-peak stapes-footplate displacements were extracted at the probe location for each excitation cycle. Mean steady-state amplitudes were computed by averaging the peak-to-peak values over several cycles once a periodic plateau had been reached. This procedure was chosen to reduce sensitivity to transient oscillations and to provide a robust measure of the steady-state mechanical response. All numerical results are provided in the manuscript and supplementary material; additional datasets are available from the corresponding author upon reasonable request.

III. RESULTS

A. Simplified model performance

Our study initially examined the mean amplitude of stapes displacement as a function of frequency and sound intensity for the simplified model, covering a frequency range from 4 Hz to 4000 Hz and intensities ranging from 70 dB to 120 dB (Fig. 1, **Supplementary table I**).

The analysis revealed a log-linear relationship between sound intensity and displacement amplitude. For each 20 dB increase (equivalent to a 100-fold increase in acoustic pressure), the amplitude increased by one order of magnitude, consistent across the entire frequency range.

At infrasound frequencies (4–20 Hz), the amplitude of stapes displacement remained relatively constant across different frequencies at a fixed sound intensity. For example, at 70 dB, the amplitude varied from 2.16×10^{-3} µm at 4 Hz to 2.18×10^{-3} µm at 20 Hz.

In the mid-frequency range, a progressive increase in mean displacement amplitude was observed, accompanied by a slow amplitude modulation pattern reaching a maximum around 1000 Hz (Fig. 4). Beyond this range, the amplitude rapidly decreased, showed a secondary rise near 2500 Hz, and then declined again toward 4000 Hz.

This modulation pattern suggests the presence of frequency-dependent dynamic behavior, consistent with the system's intrinsic vibratory modes.

B. Effect of fluid loading (FSI model)

Subsequently, our study examined the mean peak-to-peak displacement amplitude of the stapes using the fluid-structure interaction (FSI) model for specific frequencies (4 Hz, 20 Hz, 500 Hz, 1000 Hz, and 2000 Hz) at two sound intensity levels (90 dB and 110 dB). The number of frequencies and sound intensities tested was reduced due to the significantly increased computational resources required for the cochlear model simulation.

This model, like the previous one, demonstrated a proportional increase in stapes displacement amplitude by one order of magnitude between 90 dB and 110 dB (**Supplementary table II**).

At low frequencies (4 Hz and 20 Hz), the amplitude of stapes displacement remained stable. At 90 dB, the amplitude was 2.40×10^{-2} µm at 4 Hz and increased slightly to 2.42×10^{-2} µm at 20 Hz. At 110 dB, the corresponding values were 2.40×10^{-1} µm and 2.42×10^{-1} µm, respectively, representing a tenfold increase for a 20 dB increase. At 500 Hz, a slight increase in amplitude was observed. The amplitude reached 3.36×10^{-2} µm at 90 dB and 3.21×10^{-1} µm at 110 dB. In the fluid–structure interaction (FSI) model, simulations were performed for a limited number of frequencies, mainly to evaluate the influence of fluid coupling on displacement amplitude (Fig. 5).

Within this restricted range, the overall trend appeared comparable to that of the simplified solid model, with similar low-frequency stability and a modest amplitude increase toward the mid-frequency domain. A slight envelope modulation was still visible, but with reduced magnitude, suggesting that fluid loading exerted a mild damping effect without substantially modifying the overall dynamic behavior.

The peak amplitude was again observed at 1000 Hz for both intensity levels. At this frequency, the amplitude was 2.03×10^{-1} µm at 90 dB and 1.99 µm at 110 dB, representing the maximum displacement values for this model (Fig. 2).

C. Anatomical model response (Animation of the model displayed in Supplemental file 1)

Finally, our study examined the mean amplitude of stapes displacement as a function of frequency and sound intensity for the complete model, again covering a frequency range from 4 Hz to 4000 Hz and intensities ranging from 70 dB to 120 dB, as in the first simplified model (**Supplementary table III**).

The analysis also revealed a similar log-linear relationship between sound intensity and displacement amplitude across the entire frequency range (one order of magnitude in displacement amplitude for 20 dB).

In the infrasound range (4–20 Hz), the amplitude of stapes displacement remained constant for each intensity level. For example, at 70 dB, the amplitude varied from 6.33×10^{-4} µm at 4 Hz to 6.35×10^{-4} µm at 20 Hz. The frequency response exhibited the same general pattern, with low-frequency stability followed by a pronounced increase near the mid-frequency range (Fig. 6).

The amplitude envelope again displayed a slow modulation consistent with the dynamic behavior observed in previous models, although amplitude fluctuations were visible at higher frequencies, reflecting the influence of complex geometrical features.

D. Sensitivity and parametric analysis

Based on the anatomical model, a series of parametric modifications were applied to the simplified configuration at 4 and 250 Hz to evaluate their influence on stapes displacement. The sensitivity and parametric analyses were performed using the simplified model in order to enable controlled, systematic variations of individual geometric and mechanical parameters. The anatomical model, which includes spatially heterogeneous tympanic-membrane thickness and fine structural details, was subsequently used to verify whether the main trends identified in the simplified configuration persisted in a geometrically realistic setting.

Reducing the tympanic membrane diameter from 10 mm (78 mm²) to 8.75 mm (60 mm²), corresponding to a 23% reduction in surface area, led to a 27% decrease in stapes displacement amplitude (from 6.84×10^{-1} µm to 5.00×10^{-1} µm). This discrepancy in surface between anatomical and simplified models arose because the simplified model assumed a perfectly circular tympanum, whereas the real eardrum is tear-drop shaped, with a smaller effective surface than an ideal circle of equal long-axis diameter. This proportional variation indicates an almost linear relationship between tympanic diameter and stapes motion. Increasing tympanic thickness from 0.1 to 0.5 mm significantly reduced stapes displacement by approximately 50%.

Variations in contact radius between the tympanic membrane and the ossicular prosthesis or in stapes footplate surface produced negligible changes in amplitude. Modifications in footplate thickness or oval window area had negligible impact.

Reducing annular ligament height from 0.25 to 0.10 mm increased amplitude by nearly threefold. Increasing the axial thickness of the annular ligament by 25% (i.e., moving the fixation point further from

the footplate) resulted in an approximately 10% increase in stapes displacement amplitude, suggesting a moderate lever effect related to ligament geometry.

Overall, tympanic membrane geometry (diameter and thickness) and annular ligament morphology emerged as the main determinants of amplitude variance between models.

IV. DISCUSSION

A. Mechanical behavior in the infrasonic range

This comparative study of three biomechanical models of the human middle ear has revealed important characteristics of the stapes response to various frequencies and sound intensities. To situate our results within existing modeling literature, we compared the predicted stapes displacements at 1 kHz and 90 dB SPL with those reported in prior finite-element and FSI studies (**Supplemental file 5**: comparison of middle-ear models). The amplitudes obtained here (ranging from ≈ 0.03 to 0.2 µm depending on the model and loading condition) are consistent with published human data, typically ranging between 0.05 and 0.1 µm under similar conditions[15,17,21,22]. Extending these validated mechanical boundary conditions to the infrasonic range provides a quantitative continuity between classical finite-element predictions and sub-audible mechanical behavior. Although the constitutive laws were linear elastic, several excitation levels were simulated to verify that the system response remained proportional to input pressure across the investigated range and to confirm the absence of numerical or geometric nonlinearities.

The first notable result concerns the response to infrasound (frequencies below 20 Hz). All three models showed a very stable stapes displacement amplitude in this frequency range, suggesting that the middle ear maintains efficient infrasound transmission without significant amplification or attenuation. All models demonstrated an approximately tenfold increase in displacement amplitude for each 20 dB increase in sound intensity, suggesting the middle ear's ability to maintain a proportional response over a wide range of sound intensities.

The comparison between the simplified mechanical model and the fluid-structure interaction (FSI) model revealed similar results. This concordance between the simplified mechanical model and the FSI model demonstrates that, in this context, the integration of a simplified cochlear model and its resistance does not significantly alter the stapes movement.

B. Role of geometry and boundary conditions

Our findings regarding the frequency-dependent stapes response are consistent with the works of Gan et al., who reported stapes-footplate displacements on the order of 0.01–0.03 µm around 1 kHz and comparable magnitudes over the 250–2000 Hz range depending on excitation level and model assumptions[14]. The agreement between our simplified mechanical model and the fluid–structure interaction (FSI) configuration is in line with the conclusions of Gan et al. (2004), who demonstrated that

reduced-order descriptions may be adequate for selected analyses of middle-ear mechanics[13]. Our results are also consistent with the work of Nakajima et al. (2009), which showed that incorporating a simplified cochlear load can reproduce the main features of ossicular-chain dynamics, particularly at the stapes[19]. These comparisons do not constitute a full experimental validation but indicate that the predicted responses fall within the range reported for human temporal-bone measurements.

The anatomical model developed in this study revealed average displacement amplitudes that were 2 to 4 times lower than those observed in the two previous models and in the work of Gan et al. in 2004[14], but still within the same order of magnitude. Green et al. (2017) examined stapes displacement at high sound intensities (100 to 180 dB) for frequencies ranging from 20 to 2500 Hz, and reported displacements between 0.1 and 100 µm[23]. For the same frequency range (20 to 2500 Hz), the average stapes displacement in our anatomical model was between $6.34x10^{-4}$ and 1.27 µm.

The parametric analysis indicates that the geometry and stiffness of the tympanic membrane and the morphology of the annular ligament are the main determinants of stapes displacement amplitude. The nearly linear relationship observed between tympanic diameter and stapes motion reflects a direct proportionality between the effective vibrating surface and the transmitted mechanical energy. The simplified model slightly overestimated the tympanic surface area because it assumed a perfectly circular membrane based on the average human diameter (~ 10 mm), whereas the real eardrum has a tear-drop shape with a 20–25% smaller effective area. This geometric simplification accounts for part of the amplitude difference between the models, as the idealized circular surface transmits greater displacement to the ossicular chain. Tympanic thickness also emerged as a critical parameter. In the simplified model, the membrane thickness (0.1 mm) was derived from the reference values used by Gan *et al.*, while the anatomical model, obtained from micro-CT data of an iodine-stained Thiel-embalmed specimen, displayed a much thicker tympanum (~ 0.5 mm)[14,20]. The resulting two-fold reduction in stapes displacement confirms the strong influence of tympanic stiffness on mechanical transfer. However, this discrepancy may reflect both an underestimation of thickness in the simplified model and a potential overestimation in the anatomical reconstruction, as iodine impregnation and fixation procedures are known to increase tissue density and apparent wall thickness. The annular ligament also plays a significant role in modulating motion amplitude. A thinner ligament reduces fixation strength and enhances stapes mobility in a roughly proportional manner (a ligament that is 2.5 times thinner is associated with a displacement amplitude of the stapes that is three times greater), while a 25% increase in its axial thickness produced a moderate 10% rise in amplitude since the fixation point is further.

Overall, the observed differences in stapes displacement between models can mainly be attributed to the combined effects of tympanic geometry and ligament boundary conditions. This underscores the importance of incorporating accurate anatomical and material properties—particularly membrane thickness and shape—into future finite-element refinements for precise modeling of middle-ear mechanics.

C. Resonance and frequency-dependent dynamics

Although the focus of the study is on infrasonic stimulation, simulations up to 4 kHz were included to enable comparison with published middle-ear transfer functions and to verify that the models reproduced well-established mid-frequency dynamics before extrapolating to lower frequencies. Regarding the increase in displacement amplitude in the mid-frequencies, the first two models demonstrated a significant increase in stapes displacement amplitude with a peak at 1000 Hz, while the third model showed a peak at 1750 Hz. These observations suggest the existence of an apparent resonance-like behavior in the mid-frequencies, which corresponds to a crucial part of the human speech spectrum. The frequency-response peaks observed in our models are largely in agreement with the literature. Indeed, numerous studies have shown that resonance frequencies are around 1 kHz[24,25], particularly Wada et al.[25], who measured average resonance frequencies of 1.17 ± 0.27 kHz in 275 living ears. Other studies have reported resonance frequencies between 1.5 and 2 kHz[26,27]. Finally, Homma et al. showed that there are two resonance frequencies depending on ossicular movements, with a first frequency at 1.2 kHz and a second at 1.7 kHz[18], which is in line with our results.

D. Implications for cochlear hydrodynamics and drug transport

Although the simulated amplitude of stapes displacement remained nearly constant across frequencies, the total mechanical energy transmitted to the cochlea depends strongly on frequency. For a sinusoidal stimulus, the instantaneous velocity of the stapes is proportional to $2\pi fA$, and the kinetic energy and mechanical power are proportional to f^2A^2. Thus, even with similar displacement amplitudes, higher-frequency stimuli produce greater oscillation rates and higher average power transfer to the cochlear fluids. In practical terms, our model indicates that a 90 dB, 2 kHz stimulus transmits roughly an order of magnitude more mechanical power than a 130 dB, 12 Hz stimulus, despite the latter's far higher sound pressure level. This apparent paradox arises from the logarithmic nature of the decibel scale and the low oscillation rate of infrasound, which limits the total mechanical work performed per second.

However, the physical mechanisms relevant to drug transport may not depend solely on instantaneous energy flux. Infrasound stimulation, although energetically less efficient, can generate slow, large-scale perilymph displacements and steady-streaming flows due to viscous boundary layer effects, while minimally exciting the organ of Corti. This low-frequency regime may therefore favor bulk fluid movement over oscillatory energy transfer. These considerations remain speculative and are intended to provide a physical interpretation rather than a direct prediction of drug transport.

To our knowledge, the present simulations provide numerical evidence that middle-ear transmission persists into the infrasonic domain, a frequency range relevant to environmental exposure, vestibular stimulation, and emerging concepts of acoustically driven cochlear drug delivery. The results of this study may therefore motivate further investigations into low-frequency stimulation strategies, although any implications for cochlear drug delivery remain speculative and should be viewed as a long-term perspective rather than as a demonstrated outcome of the present simulations.

E. Methodological limitations and perspectives

This study has several limitations. First, the precise extraction of anatomical models remains a persistent challenge for all ear models. Although high-resolution micro-computed tomography (μCT) has greatly improved geometric accuracy, some approximations remain unavoidable. Second, determining the mechanical properties of middle-ear tissues and ligaments remains difficult, as most parameters cannot be measured in vivo and are often extrapolated from animal data, requiring careful translation to the human scale. The ossicular joints were represented as continuous linear elastic connections rather than modeled explicitly in the anatomical model, which is a simplification. However, clinical experience, particularly from ossiculoplasty with cement, suggests that these joints have a marginal role in acoustic transmission.

Although finite-element formulations dominate middle-ear modeling, we adopted a finite-volume approach because it ensures strict local conservation of momentum and energy at fluid–solid interfaces and allows a fully coupled treatment of acoustics and structural dynamics within a single framework. Studies have shown that FVM can achieve frequency-domain accuracy comparable to FEM when time-step and mesh-resolution criteria are satisfied[28,29]. In the present study, time steps were selected to provide at least 200 points per excitation period, and mesh densities were locally refined in thin structures such as the tympanic membrane and annular ligament to limit numerical dispersion.

Another limitation relates to the computational cost associated with high-resolution finite-volume and fluid–structure interaction modeling. To ensure numerical feasibility while adequately resolving infrasonic stimulation, simulation duration was adapted to the excitation frequency, with time windows long enough to include multiple oscillation cycles. In particular, for the lowest frequency investigated (4 Hz), simulations were extended over several seconds to capture more than ten acoustic periods and ensure convergence toward a steady-state harmonic response. The present simulations were designed to characterize frequency-dependent steady-state acoustic transmission under harmonic pressure excitation rather than long-term non-periodic dynamics. Solver-related factors may also have influenced the results. The segregated finite-volume solver implemented in Star-CCM + is well suited for small-deformation analyses but may introduce a limited amount of numerical damping, particularly at higher frequencies. The chosen time-step and relaxation parameters ensured numerical stability but could have attenuated resonance amplitude. Moreover, mesh convergence was assessed qualitatively rather than through a full mesh-independence study. Future work could therefore benefit from systematic mesh and time-step convergence analyses and, where feasible, alternative coupling strategies to further improve numerical accuracy while maintaining computational efficiency.

V. CONCLUSION

This comparative study of three biomechanical models of the human middle ear suggests that infrasonic stimuli induce stapes displacements comparable to those observed at audible frequencies,

supporting a continuous mechanical response across the spectrum. These findings provide a robust foundation for future modeling of cochlear fluid dynamics.

The present results establish boundary-condition data for upcoming computational studies of cochlear hydrodynamics, enabling simulation of fluid and particle transport driven by stapes motion in the infrasonic range.

Future work should integrate full cochlear geometry and higher temporal resolution to characterize resonance modes and their influence on cochlear fluid motion. Such developments could ultimately support novel strategies for targeted inner-ear drug delivery.

Declarations

Declaration of competing interest:

The author declares no competing financial interests or personal relationships that could influence the work reported in this paper.

Ethics approval:

Not applicable. This study did not involve human participants or animals.

Funding:

This research received no specific grant from any funding agency in the public, commercial, or not-for-profit sectors.

Author Contribution

IO: Performed the numerical simulations, contributed to data analysis, and participated in manuscript drafting.RH: Assisted in model preparation, parameter definition, and result validation.LM: Developed the computational pipeline and supervised the numerical optimization steps.TR: Contributed to study conception, data interpretation, and critical manuscript revision.JM: Provided clinical supervision, validated anatomical modeling, and critically reviewed the final version of the manuscript.SH: Provided the anatomical datasets and contributed to model reconstruction and figure design.DE: Participated in data organization, figure preparation, and manuscript editing.SG: Conceived and designed the study, coordinated the project, interpreted the results, and wrote the manuscript

Acknowledgement

Centre de Calcul Intensif d’Aix-Marseille is acknowledged for granting access to its high-performance computing resources.

Data Availability

All data is available within the manuscript

References

1. Vos 1T et al (2017) Global, regional, and national incidence, prevalence, and years lived with disability for 328 diseases and injuries for 195 countries, 1990–2016: a systematic analysis for the Global Burden of Disease Study 2016. Lancet 390:1211–1259. 10.1016/S0140-6736(17)32154-2
2. Nyberg 2S (2019) Delivery of therapeutics to the inner ear: The challenge of the blood-labyrinth barrier. Sci Transl Med 11:eaao0935. 10.1126/scitranslmed.aao0935
3. Smith 3RJ (2005) Sensorineural hearing loss in children. Lancet 365:879–890. 10.1016/S0140-6736(05)71047-3
4. Rivera 4T (2012) Drug Delivery to the Inner Ear: Strategies and Their Therapeutic Implications for Sensorineural Hearing Loss. CDD 9:231–242. 10.2174/156720112800389098
5. Salt 5AN, and (2009) Principles of Local Drug Delivery to the Inner Ear. Audiol Neurotol 14:350–360. 10.1159/000241892
6. Salt 6AN (1986) Direct measurement of longitudinal endolymph flow rate in the guinea pig cochlea. Hear Res 23:141–151. 10.1016/0378-5955(86)90011-0
7. Schilder 7AGM et al (2019) Hearing Protection, Restoration, and Regeneration: An Overview of Emerging Therapeutics for Inner Ear and Central Hearing Disorders. Otology Neurotology 40:559–570. 10.1097/MAO.0000000000002194
8. Ungar 8OJ (2024) Sound Exposure Promotes Intratympanic Drug Delivery to the Inner Ear. Otolaryngol --head neck surg 171:1133–1139. 10.1002/ohn.801
9. Sumner 9L (2021) Steady streaming as a method for drug delivery to the inner ear. Sci Rep 11:57. 10.1038/s41598-020-79946-z
10. Edom 10E (2014) Steady streaming in a two-dimensional box model of a passive cochlea. J Fluid Mech 753:254–278. 10.1017/jfm.2014.360
11. Flaherty 11SM (2021) Drug distribution along the cochlea is strongly enhanced by low-frequency round window micro vibrations. Drug Delivery 28:1312–1320. 10.1080/10717544.2021.1943059
12. Gan 12RZ (2006) Acoustic–structural coupled finite element analysis for sound transmission in human ear—Pressure distributions. Med Eng Phys 28:395–404. 10.1016/j.medengphy.2005.07.018
13. Gan 13RZ (2004) Otology Neurotology 25:423–435. 10.1097/00129492-200407000-00005. Human Middle Ear Transfer Function Measured by Double Laser Interferometry System:,

14. Gan 14RZ (2004) Three-Dimensional Finite Element Modeling of Human Ear for Sound Transmission. Ann Biomed Eng 32:847–859. 10.1023/B:ABME.0000030260.22737.53
15. Ebrahimian 15A (2023) Inaccuracies of deterministic finite-element models of human middle ear revealed by stochastic modelling. Sci Rep 13:7329. 10.1038/s41598-023-34018-w
16. Zhao 16F (2009) Finite element analysis of the middle ear transfer functions and related pathologies. Med Eng Phys 31:907–916. 10.1016/j.medengphy.2009.06.009
17. Gan 17RZ (2007) Modeling of Sound Transmission from Ear Canal to Cochlea. Ann Biomed Eng 35:2180–2195. 10.1007/s10439-007-9366-y
18. Homma 18K (2009) Ossicular resonance modes of the human middle ear for bone and air conduction. J Acoust Soc Am 125:968–979. 10.1121/1.3056564
19. Nakajima 19HH (2009) Differential Intracochlear Sound Pressure Measurements in Normal Human Temporal Bones. JARO 10:23–36. 10.1007/s10162-008-0150-y
20. Halm 20S (2021) Micro-CT imaging of Thiel-embalmed and iodine-stained human temporal bone for 3D modeling. J Otolaryngol - Head Neck Surg 50:33. 10.1186/s40463-021-00522-0
21. O'Connor 21KN (2017) The effects of varying tympanic-membrane material properties on human middle-ear sound transmission in a three-dimensional finite-element model. J Acoust Soc Am 142:2836–2853. 10.1121/1.5008741
22. Golabbakhsh 22M (2023) Finite-Element Modelling Based on Optical Coherence Tomography and Corresponding X-ray MicroCT Data for Three Human Middle Ears. J Assoc Res Otolaryngol 24:339–363. 10.1007/s10162-023-00899-x
23. Greene 23NT (2017) Stapes displacement and intracochlear pressure in response to very high level, low frequency sounds. Hear Res 348:16–30. 10.1016/j.heares.2017.02.002
24. Silman 24S, and (1991) Auditory diagnosis: principles and applications. Academic, San Diego
25. Wada 25H (1998) Clinical Applicability of the Sweep Frequency Measuring Apparatus for Diagnosis of Middle Ear Diseases. Ear Hear 19:240–249. 10.1097/00003446-199806000-00007
26. Reinfeldt 26S (2007) Examination of bone-conducted transmission from sound field excitation measured by thresholds, ear-canal sound pressure, and skull vibrations. J Acoust Soc Am 121:1576–1587. 10.1121/1.2434762
27. Berger 27EH (2003) Hearing protection: Surpassing the limits to attenuation imposed by the bone-conduction pathways. J Acoust Soc Am 114:1955–1967. 10.1121/1.1605415
28. Xuan 28L (2014) Time domain finite volume method for three-dimensional structural–acoustic coupling analysis. Appl Acoust 76:138–149. 10.1016/j.apacoust.2013.07.024
29. Lopes 29D (2021) Analysis of finite element and finite volume methods for fluid-structure interaction simulation of blood flow in a real stenosed artery. Int J Mech Sci 207:106650. 10.1016/j.ijmecsci.2021.106650

Figures

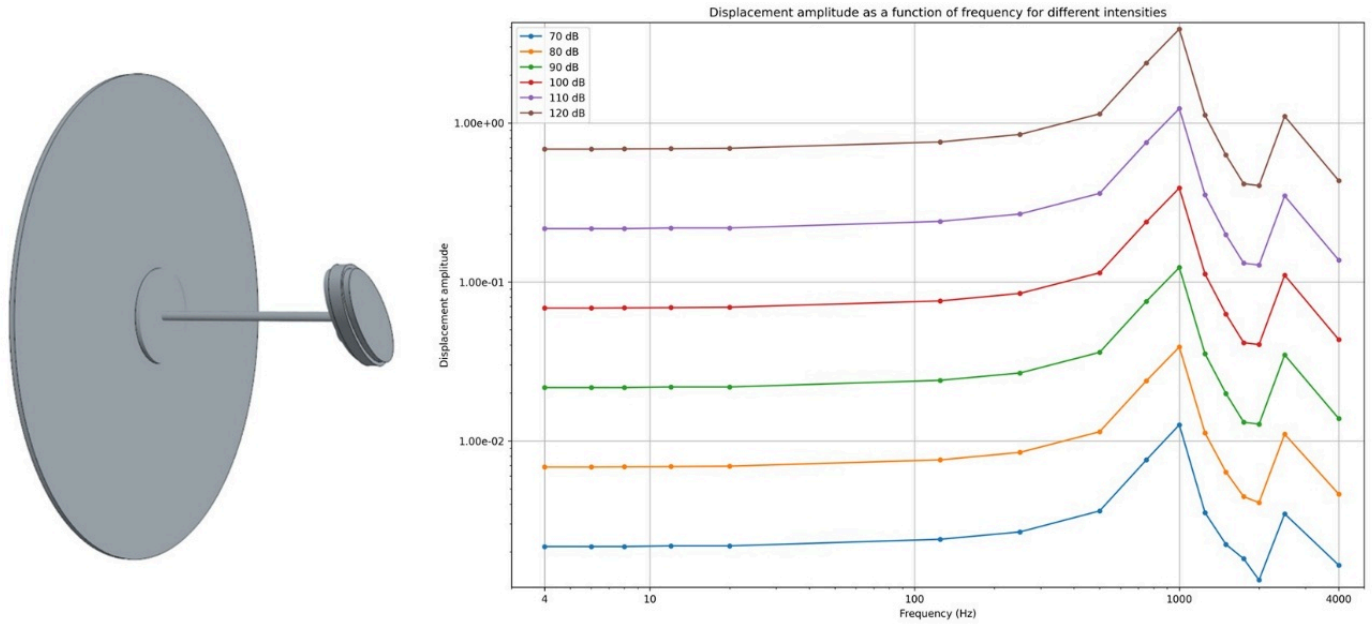


Figure 1

Simplified model: Star-CCM+ geometry (left) and stapes displacement (in μm) as a function of frequency and intensity (right).

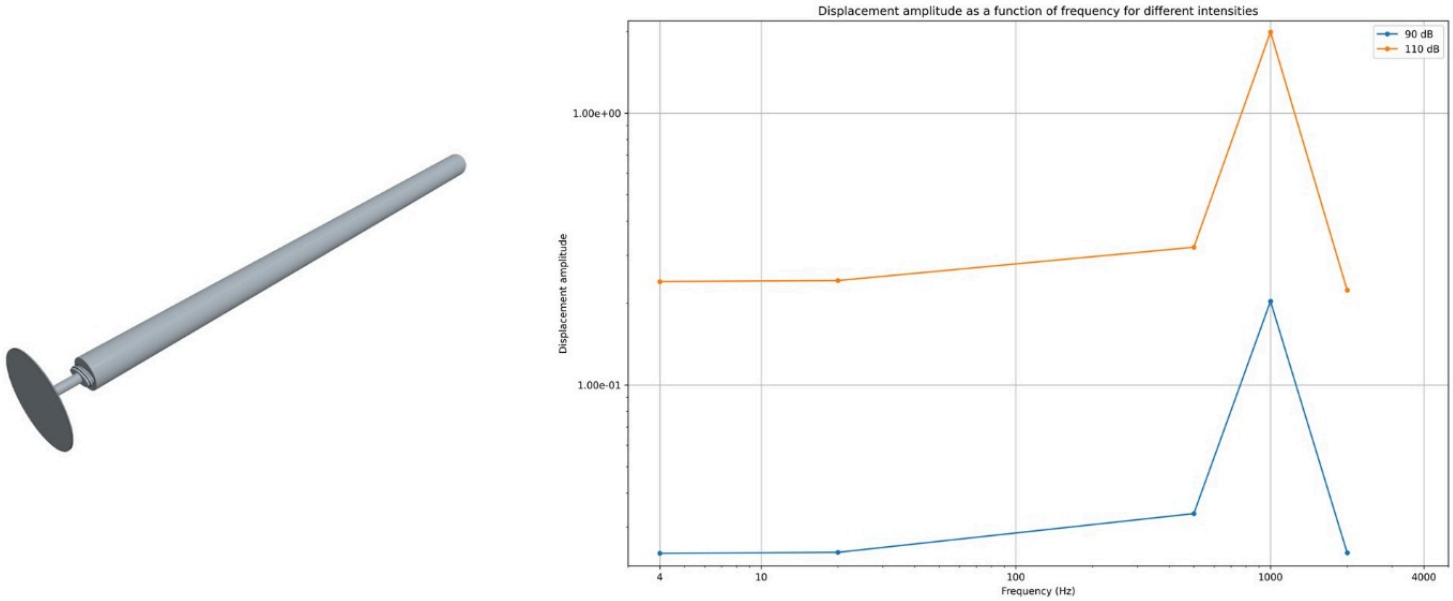


Figure 2

Fluid–structure interaction (FSI) model: Star-CCM+ geometry (left) and stapes displacement (in μm) as a function of frequency and intensity (right).

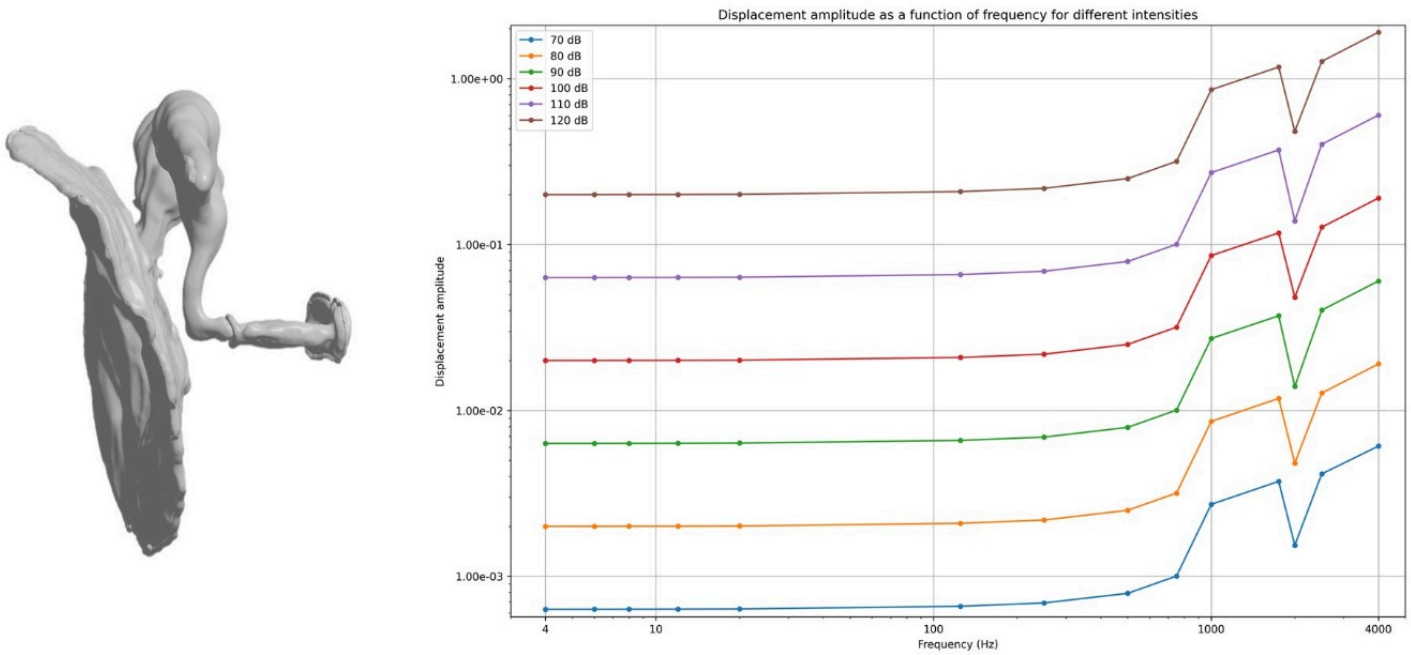


Figure 3

Anatomical model: Star-CCM+ geometry (left) and stapes displacement (in μm) as a function of frequency and intensity (right).

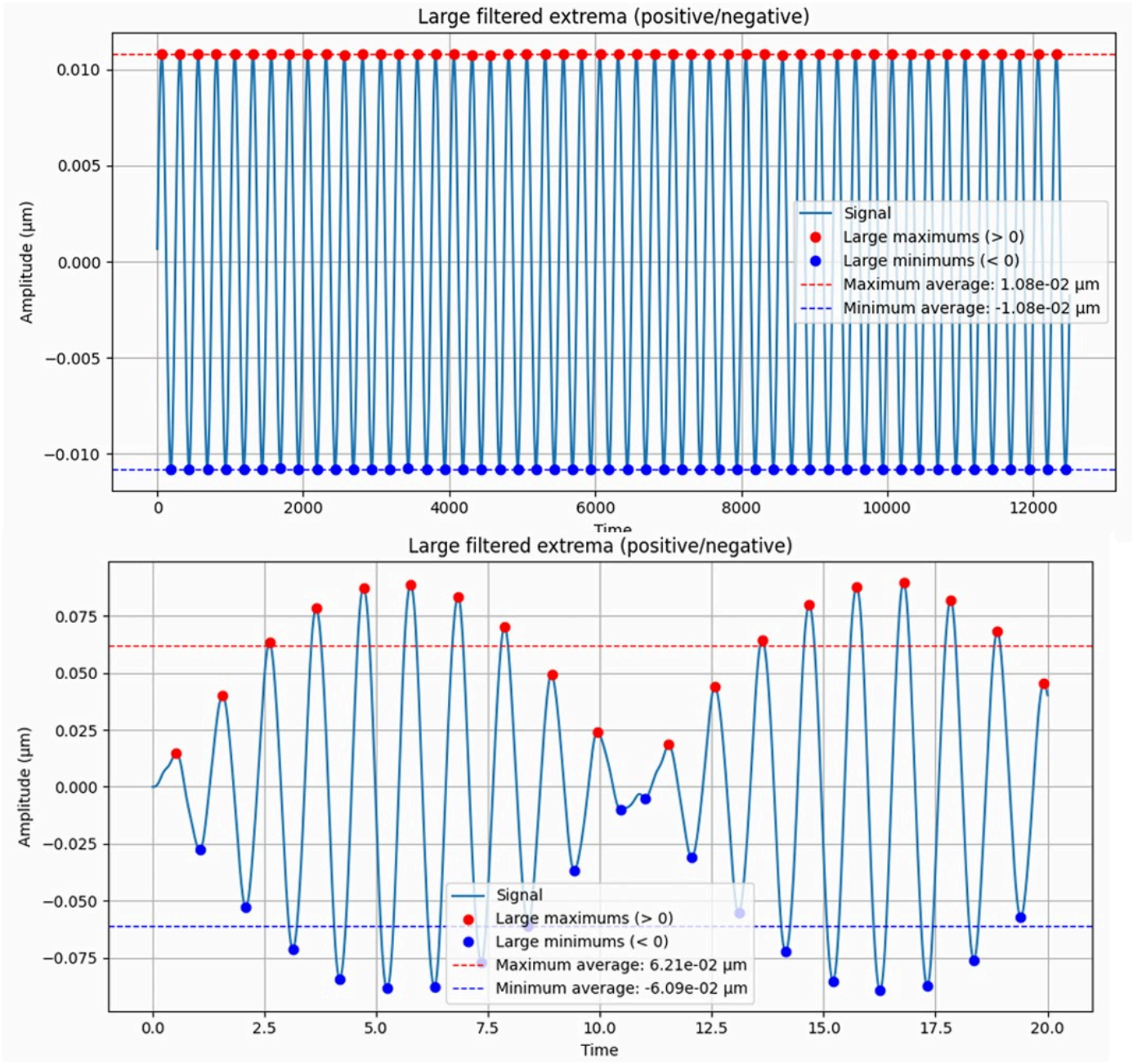


Figure 4

Simplified model: Average displacement amplitude maps at 4 Hz (upper) and 1000 Hz (lower) for 90 dB SPL stimulation.

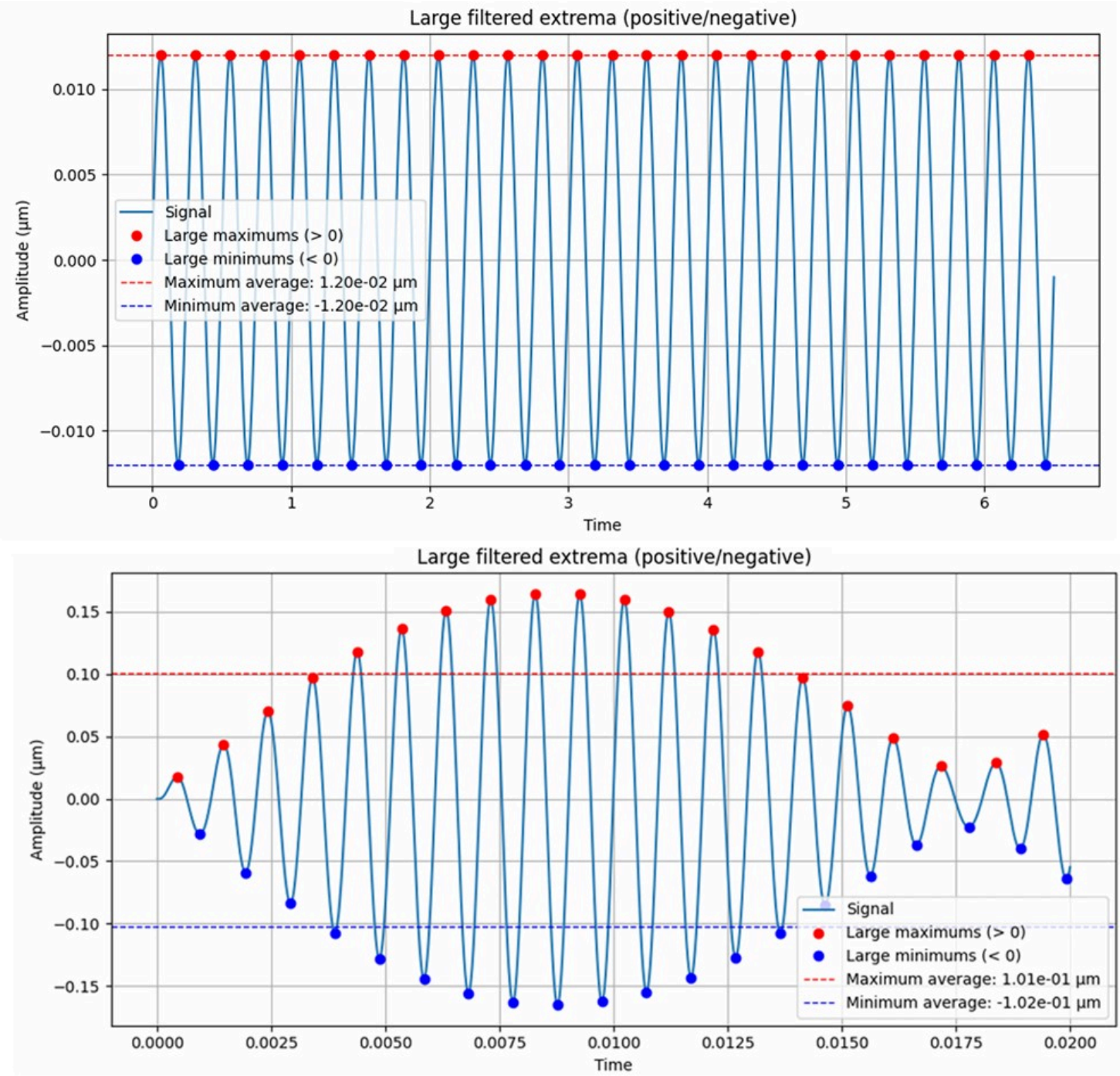


Figure 5

FSI model: Average displacement amplitude maps at 4 Hz (upper) and 1000 Hz (lower) for 90 dB SPL stimulation.

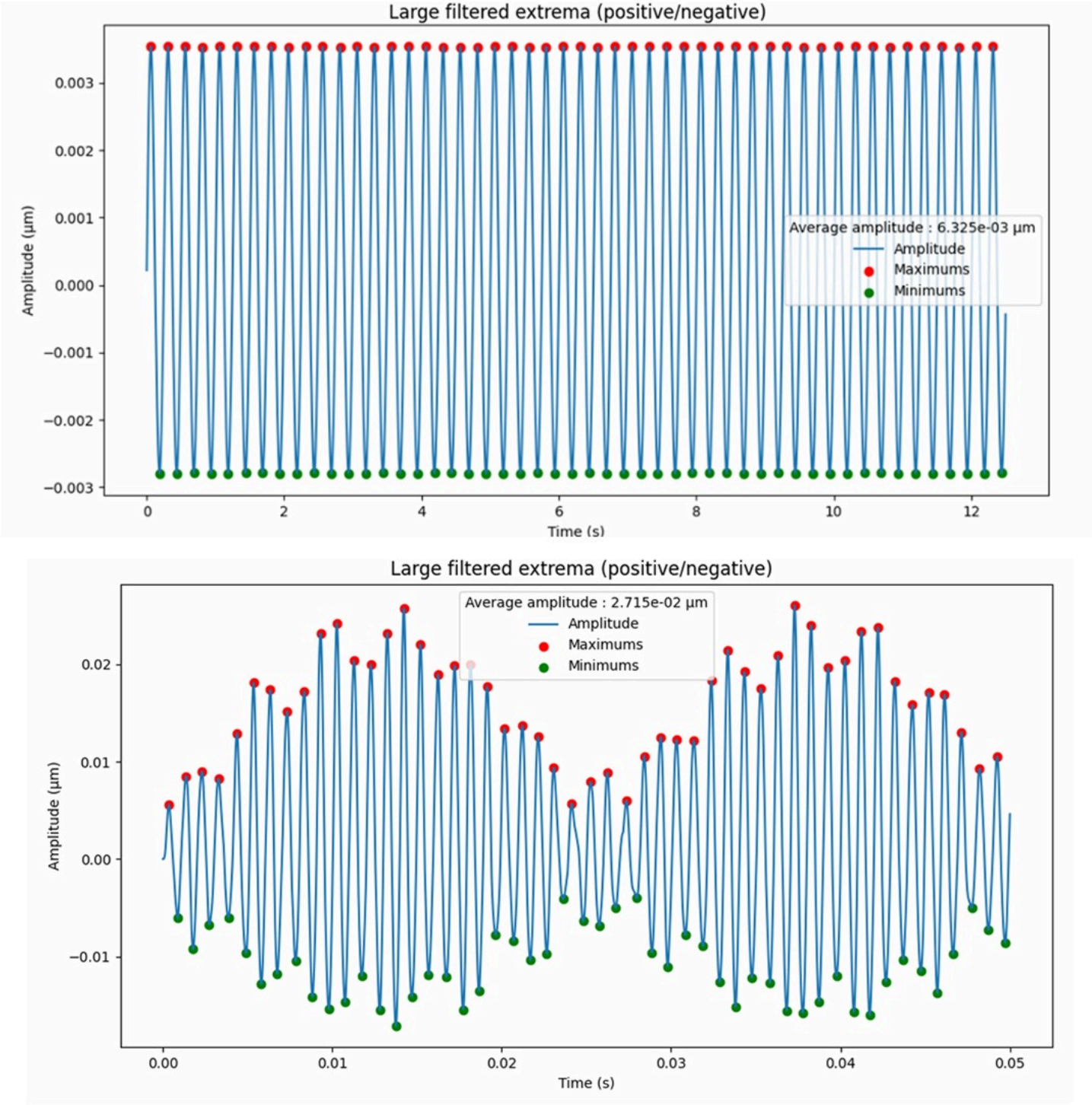


Figure 6

Anatomical model: Average displacement amplitude maps at 4 Hz (upper) and 1000 Hz (lower) for 90 dB SPL stimulation.

Supplementary Files

This is a list of supplementary files associated with this preprint. Click to download.

- SUPPLEMENTALFILES.docx
- SupplementalfileIVAnatomicalmodelanimation.mp4
- SupplementalfileVTableComparisonofMiddleEarModels.docx